

Article

Enhanced Tunable Properties of Strontium Barium Niobate Films on Dielectric Alumina Substrate at Microwaves

Andrey Tumarkin ^{1,*}, Alexey Bogdan ¹, Evgeny Sapego ¹, Alexander Gagarin ¹, Ludmila Ivleva ², Igor Serenkov ³ and Vladimir Sakharov ³

¹ Department of Physical Electronics and Technology, Saint Petersburg Electrotechnical University "LETI", 197022 Saint Petersburg, Russia; aggagarin@etu.ru (A.G.)

² Alexander Mikhailovich Prokhorov Institute of General Physics, Russian Academy of Sciences, 119991 Moscow, Russia; ivleva@lst.gpi.ru

³ Abram Fedorovich Ioffe Institute of Physics and Technology, Russian Academy of Sciences, 194021 Saint Petersburg, Russia

* Correspondence: avtumarkin@yandex.ru

Abstract: (Sr,Ba)Nb₂O₆ (SBN) relaxor ferroelectric thin films exhibiting nonlinear properties promising for microwave applications were grown on a polycrystalline aluminum oxide substrate for the first time. Films of good crystallinity were obtained using the sputtering technique and high-temperature annealing. For all films, a significant change in the phase composition after high-temperature treatment was observed, and annealing provided a different effect on the phase composition of films deposited at different substrate temperatures. Tunable properties of the SBN films were investigated as a function of the deposition temperature and annealing conditions using planar capacitors with microwaves. The capacitor based on the strontium barium niobate film deposited at a temperature of 950 °C and subjected to annealing demonstrates a tunability of 44% and a loss tangent of 0.009 ÷ 0.022, which is expressed in the microwave commutation quality factor of 1740. This is the first successful attempt to form planar capacitive structures based on SBN films, which reveal a commutation quality factor above 1000 for tunable microwave applications.



Citation: Tumarkin, A.; Bogdan, A.; Sapego, E.; Gagarin, A.; Ivleva, L.; Serenkov, I.; Sakharov, V. Enhanced Tunable Properties of Strontium Barium Niobate Films on Dielectric Alumina Substrate at Microwaves. *Coatings* **2023**, *13*, 1937. <https://doi.org/10.3390/coatings13111937>

Academic Editor: Aomar Hadjadj

Received: 20 October 2023

Revised: 10 November 2023

Accepted: 13 November 2023

Published: 14 November 2023



Copyright: © 2023 by the authors. Licensee MDPI, Basel, Switzerland. This article is an open access article distributed under the terms and conditions of the Creative Commons Attribution (CC BY) license (<https://creativecommons.org/licenses/by/4.0/>).

Keywords: ferroelectrics; microwave properties; strontium barium niobate; electrical tuning

1. Introduction

Ferroelectrics (FE) are characterized by a strong dependence of the dielectric permittivity on the external electric field, which makes them potential candidates for use in tunable microwave devices. Capacitors, delay lines, filters, and phase shifters can be realized on the basis of ferroelectric materials [1–3]. To implement FE microwave devices, a functional material is needed, which simultaneously exhibits high dielectric nonlinearity and a low level of losses at microwaves. The search for such a material stimulates the study of various ferroelectrics at frequencies above 1 GHz. Dielectric and tunable properties of ferroelectric solid solutions of lead zirconate titanate [4], barium zirconate titanate [5], and barium stannate titanate [6] have already been studied. The most investigated ferroelectric solid solution for microwave applications is considered to be strontium barium titanate Ba_xSr_{1-x}TiO₃ (BST) [7]. At the same time, there are a number of ferroelectric materials where, instead of titanium, other metal ions act as the key ion of the unit cell. It is known that the nonlinear reaction of the dielectric permittivity of ferroelectrics to an external electric field is due to the displacement of the central cation relative to the oxygen octahedron. The radius of this ion directly affects the dielectric properties of the ferroelectric material. In this case, strontium barium niobate Sr_xBa_{1-x}Nb₂O₆ (SBN) looks more attractive compared to BST in terms of the dielectric nonlinearity, since the smaller niobium ion provides a greater ionic displacement than the titanium one ($R_{\text{Nb}} = 0.69 \text{ \AA} < R_{\text{Ti}} = 0.75 \text{ \AA}$) [7,8]. In addition, strontium barium niobate in thin film form exhibits high permittivity values at

relatively low losses at microwaves [9], which makes it promising as a nonlinear material of tunable microwave devices.

To date, multicomponent oxide films of high structural perfection on various substrates have been obtained using laser deposition [10], chemical vapor deposition [11], physical sputtering of stoichiometric targets [12,13], liquid phase epitaxy [14], and sol-gel technology [15,16]. However, it should be noted that thin films, including epitaxial ones, often exhibit worse electrical properties compared to a bulk crystal [17]. The reasons for the decrease in dielectric nonlinearity, deterioration of losses, and increase in leakage current of thin films may be a dead layer on the film–substrate interface [18], internal stresses in epitaxial films [19], and poor electrical conductivity of oxide-conducting electrodes [20]. To improve the electrical characteristics of FE films, high-temperature annealing of deposited films [21,22], strain engineering [23,24], and structuring of FE layers are used [25,26]. However, despite the fact that epitaxial FE films are confidently formed on structurally matched monocrystalline substrates such as MgO, SrTiO₃, and LaAlO₃, the best microwave characteristics, which have not been improved to date, have been demonstrated on polycrystalline films deposited by the magnetron sputtering technique [27,28].

It is known that strontium barium niobate has excellent electro-optical, pyroelectric, and photorefractive properties. There are many publications devoted to the above-mentioned properties of SBN, summarized, for example, in reviews [29,30]. At the same time, much fewer articles are devoted to the study of the dielectric and tunable properties of strontium barium niobate [31]. Today, studies on the dielectric properties of SBN films grown on silicon [32,33], magnesium oxide [9,34], and strontium titanate substrates [35,36] have been published. The vast majority of the mentioned publications provide data on the dielectric properties of SBN films in the frequency range of 1–100 kHz. Moreover, the high dielectric nonlinearity (more than 40% tunability) in these works is demonstrated exclusively in plane-parallel capacitive structures [33,34], which cannot be used at a high level of operating power [37].

In the few works dedicated to the growth of SBN layers on dielectrics, as well as the study of their microwave properties [9,38], single-crystal MgO and LaAlO₃ are used as substrates. The choice of substrates similar in structure to the deposited material makes it possible to obtain oriented films; however, both lanthanum aluminate and magnesium oxide are not optimal substrates for microwave applications: LaAlO₃ due to high cost and anisotropy of properties, and MgO due to hygroscopicity and degradation of properties over time. In addition, the planar capacitive structures formed in these studies demonstrate relatively low tunability values from 10 to 35%. Therefore, additional investigations are required to obtain SBN thin films of high tunability on a dielectric substrate. As one of such substrate material, polycrystalline aluminum oxide Al₂O₃ can be considered. Alumina is a commercially used substrate that has excellent mechanical and dielectric properties, a thermal coefficient of linear expansion close to SBN one, low losses at microwaves ($\delta < 10^{-4}$ at 10 GHz), and extremely low cost [39]. According to our data, today, there is no information in the literature about successful attempts to grow SBN films with dielectric properties acceptable for microwave applications on alumina substrate.

In this connection, the aim of this work is to investigate the technological conditions in which the growth of thin strontium barium niobate films with high tunable properties on an alumina substrate is possible, to study the structural properties of the films depending on growth conditions, and the electrical properties of SBN planar capacitors, with the purpose of their further application in electrically tunable microwave devices.

2. Experimental

2.1. Sample Preparation

The deposition of SBN films was carried out by the radio frequency magnetron sputtering of a ceramic target of the composition Sr_{0.75}Ba_{0.25}Nb₂O₆ on alumina substrates. The target was made from a mixture of pre-synthesized barium and strontium niobates at the St. Petersburg Institute “Ferrite-Domain”. Chemically pure powders BaNb₂O₆ and SrNb₂O₆

synthesized at the Moscow Institute of General Physics were used as starting materials for the target preparation. The film deposition conditions were as follows: the target surface was cleaned of contamination by sputtering away from the substrate; the temperature of the substrate T_s was varied in the range of 650–950 °C; and the substrate was heated by a resistive heater. Pure oxygen was used as the working gas, since during the crystallization of an SBN-type structure in gas mixtures, a deficiency of oxygen may occur with the formation of oxygen vacancies, which negatively affects the dielectric characteristics [34]. The working gas pressure P was ranged from 2 to 10 Pa. The deposition time of island films was 60 s at a working gas pressure of 10 Pa. Solid SBN films were deposited for 4 h, and the thickness of the films was 600 nm. The deposition of the solid films was started at 10 Pa, which was reduced until 2 Pa for the first 30 min of growth. After the deposition process was completed, the films were annealed in air at atmospheric pressure for 60 min at an annealing temperature of $T_{an} = 1000$ °C.

2.2. Structure Investigation

The beginning stages of the formation of SBN films were studied by the method of scattering medium-energy ions (MEIS). To determine the structure of the island films, the surface of the samples was bombarded with a monoenergetic flow of helium ions with an energy of 227 keV. Spectra of backscattered He^+ ions were obtained for island films investigated. By comparing experimental and model spectra, the geometric dimensions of the islands, the area of the substrate covered by islands, and the elemental content of the films were determined.

The phase composition of the obtained SBN films was monitored using X-ray diffraction phase analysis (XRD) on a DRON-6 diffractometer using $CuK\alpha$ radiation (1.54 Å). Measurements were carried out in continuous mode at diffraction angles from 20° to 60° with a scanning speed of 2°/min. Crystal phases were identified using the PDF-2 powder diffraction database. The elemental composition of the samples and the uniformity of the component distribution were studied by scanning electron microscopy (SEM) on a Teskan Mira 3 microscope using a scintillation-type detector of reflected electrons. To remove the induced charge from the dielectric surface, a thin layer of carbon was deposited onto the surface under study. The elemental composition was analyzed in real time using an integrated energy dispersion spectrometer (EDS).

2.3. Electrical Measurements

For electrophysical measurements, planar capacitive structures were formed on the base of SBN films. To form a capacitor, a layer of copper with an adhesive chromium sublayer was applied to the surface of the SBN film by thermal evaporation in vacuum. The configuration of the electrodes with a gap width of 5 μm was formed by photolithography and chemical etching. Capacitance C and quality factor $Q = 1/\tan \delta$ of capacitors were measured at 2 GHz using a half-wave strip resonator. The unloaded Q -factor of the resonator was 1000, ensuring the accuracy of capacitance and Q -factor measurements of 1% and 5%, respectively. The resonator design provides the ability to supply a control voltage up to 1000 V. Bias voltage applied to a capacitor was varied within 0–300 V that corresponded to a control field strength of $E \approx 0$ –60 V/ μm . The tunability of the capacitors was calculated as the ratio of capacitances at zero and the maximum applied control electric field strength $n = C_{max}(0 \text{ V}/\mu m)/C_{min}(E_{max})$, and additionally as $n = (C_{max} - C_{min})/C_{max}$.

3. Results and Discussion

3.1. Initial Stages of SBN Film Growth

The source of important information necessary for understanding the mechanisms of thin film growth is found in the study of the initial stages of their formation. It is known that the conditions under which the film originates on the substrate significantly affect the orientation and dimensions of the crystallites, stoichiometry, and the presence of inclusions of secondary phases [25,26]. The mechanisms of mass transfer at the initial stage of film

growth, which are key in understanding the nucleation and formation of films as a whole, are determined by the lifetime of adatoms on the substrate surface. In turn, this parameter can vary widely depending on the supersaturation, the temperature of the substrate, its structure, and its composition [27]. The geometric shape of the islands and the area of the substrate covered by islands provides data about the mechanisms of mass transfer of sputtered atoms and about the prevailing mechanisms of island growth under certain technological conditions. For example, an increase in the average height of the islands with a simultaneous reduction in the substrate area occupied by them points to a change in the mechanism of mass transfer from the surface diffusion to the diffusion through the gaseous phase, and, hence, indicates a change in the mechanism film growth from “layer-by-layer” to “island” one [40].

The energy spectra of backscattered He^+ ions from SBN island films grown in an oxygen atmosphere at T_s of 750–950 °C are presented in Figure 1. The spectra obtained from films deposited at different substrate temperatures do not have significant differences, which indicates a similar form of the SBN islands on the substrate surface and, therefore, indicates similar mechanisms of their nucleation. The sections of the spectra corresponding to the scattering of helium ions on Ba, Sr, and Nb have a triangular shape, which corresponds to the pyramidal shape of the islands [41]. Data on the technological conditions and on the structure of the island SBN films are given in Table 1. Here, τ is the deposition time; X_{med} is the average height of the island; C is the area of the substrate occupied by island film; and A is the total quantity of $\text{SrBaNb}_2\text{O}_6$ substance on a substrate in units of 10^{15} united atoms per cm^2 , where the united atom is a molecule of $\text{Sr}_a\text{Ba}_b\text{Nb}_c\text{O}_d$ and $(a + b + c + d) = 1$. The intensity of the reflexes of Ba and Sr + Nb (strontium and niobium are indistinguishable by MEIS due to the proximity of the masses) is connected with the area of substrate filled by the islands; the breadth of the reflexes is defined by the height of the islands; and the ratio of amplitudes is determined by the content of the elements in the film. The component content in island films estimated by the medium-energy ion scattering technique matches the composition of the sputtered target with a precision of 5%.

The MEIS analysis data show that the thickness of the SBN island films deposited at temperatures 750–950 °C ranges from 1.3 to 2.16 nm, the degree of substrate area covered by islands ranges from 23% to 42%, and both parameters do not correlate with the change in substrate temperature. Hence, due to the insignificant height of the islands and rather large area of the substrate occupied by them, it can be concluded that a mixed type of mass transfer prevails in this temperature range—both on the surface of the substrate and through the gas phase [42]. Based on theoretical concepts about the initial stages of growth of multicomponent films and on the MEIS analysis data, we can conclude that in the SBN system, during the condensation of sputtered atoms on the surface of a polycrystalline aluminum oxide substrate, the main mechanism of film nucleation and growth is the Volmer–Weber island regime [40]. This type of growth occurs when the atoms of the deposited substance are bonded to each other more strongly than to the substrate. In this regime, small nuclei of the condensed phase form directly on the surface of the substrate without the formation of transition layers and grow, turning into large islands [43]. In addition, during film growth on alumina, substrate defects significantly increase the rate of nucleation, reducing the height of the activation barrier, which leads to rapid filling of the substrate with islands of low height [44]. This mechanism of growth of FE films occurs, as a rule, on polycrystalline substrates that are not structure-forming for the growing film, which subsequently leads to the formation of a polycrystalline layer [41,45].

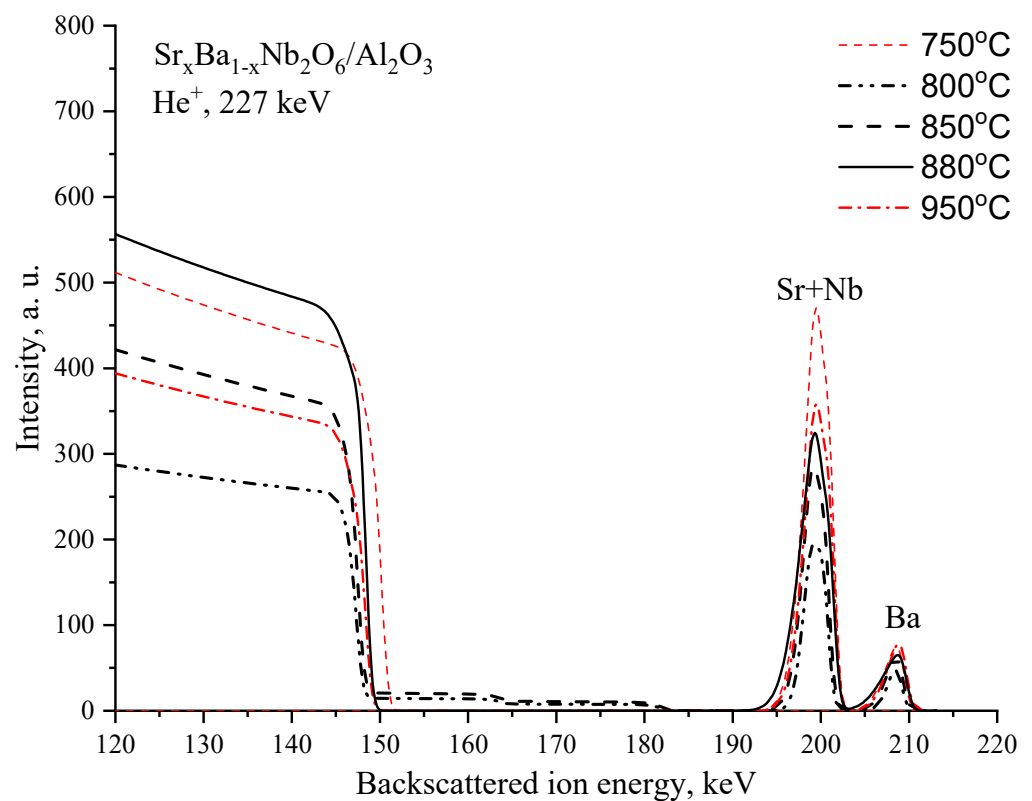


Figure 1. Spectra of backscattered He^+ ions from SBN films grown at T_s of 750–950 °C on alumina substrates.

Table 1. Characteristics of island films investigated.

No.	Substrate	T_s , °C	P , Pa	τ , s	X_{med} , nm	C , %	A
2449	Al_2O_3	850	10	60	1.29	36	3.1
2450	Al_2O_3	800	10	60	0.48	40	1.3
2452	Al_2O_3	750	10	60	1.68	42	4.7
2453	Al_2O_3	880	10	60	2.16	23	3.3
2454	Al_2O_3	950	10	60	1.56	42	4.3

3.2. Structure Characterization of SBN Films

The electrical characteristics of planar capacitive structures significantly depend on the quality of the film surface on which the capacitor electrodes will be formed. The developed morphology of the surface of the functional layer can lead to defects at the lithography and chemical etching stages, namely, the etching defects and micro-closures in the gap of the capacitor, which, finally, are common causes of electrical breakdown. To control these defects, the surface quality must be monitored on areas comparable to the area of the planar gap. For these purposes, the morphology of the surface of deposited SBN films was studied by electron microscopy. Figure 2 shows typical micrographs of the surface of films deposited at different substrate temperatures, indicating the areas of energy dispersion elemental analysis. According to the SEM analysis data, the coatings are fairly uniform and homogeneous; however, in the case of film deposition at low substrate temperatures, obvious defects in the form of cracks are observed on its surface. The situation improves when the substrate is heated to a temperature of 850 °C and above. The reason for the change in surface quality with an increase in deposition temperature may be the different phase composition of films deposited at different T_s , which will be discussed below.

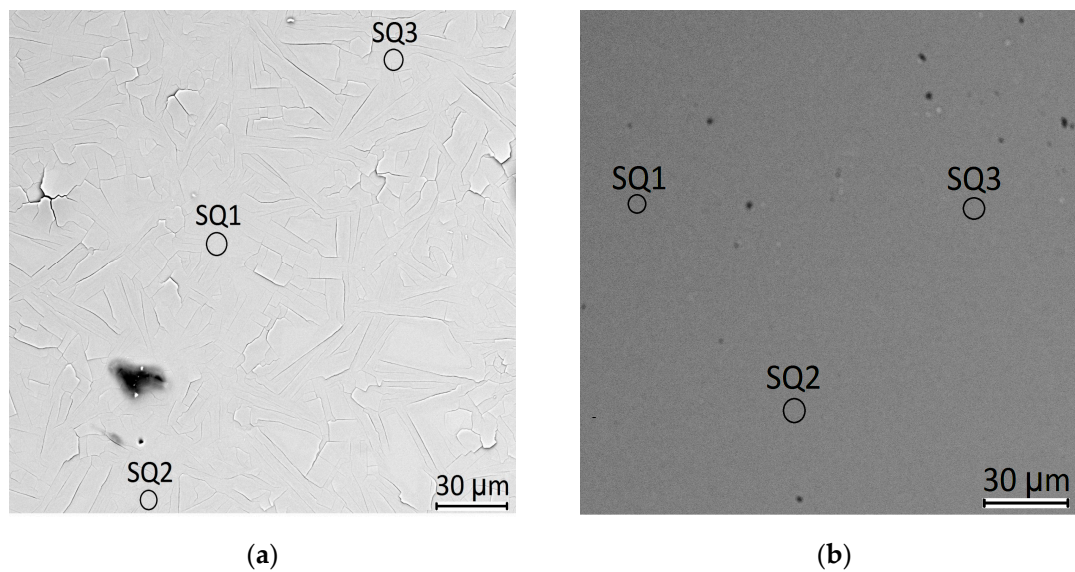


Figure 2. SEM images and areas of elemental analysis of the SBN film surface: (a) the film was deposited at 750 °C; (b) the film was deposited at 850 °C.

The elemental composition of the studied films according to the EDS analysis is presented in Table 2. The data are calculated from the reference values of Nb in the chemical SBN formula, taking into account the component composition of the target. The results of the elemental analysis of the studied films indicate the stoichiometric transfer of sputtered atoms to the substrate and a slight deviation of the Sr/Ba ratio in the film relative to the composition of the target (within 5%). A change in the substrate temperature does not lead to significant changes in the elemental composition of the deposited films. Minor deviations of the numerical ratios of Sr and Ba are noted at randomly selected analyzed surface points, explained by the chaotic surface migration of atoms along the substrate surface before and during the formation of chemical bonds [34]. A reliable assessment of the oxygen content in the studied films is difficult due to the small thickness of the films and the presence of oxygen in the substrate.

Table 2. Elemental composition of thin SBN films.

T_s , °C	Scanning Area	Atom %			
		Sr	Ba	Nb	O
750	SQ1	11.5	3.1	28.6	56.1
	SQ2	12.6	3.4	31.4	52.1
	SQ3	12.0	3.1	29.9	54.4
850	SQ1	10.8	3.0	26.5	59.2
	SQ2	10.7	3.0	26.5	59.3
	SQ3	11.3	3.0	27.9	57.6

Comparative diffractograms of thin SBN films deposited at different substrate temperatures on alumina are shown in Figure 3. Vertical dotted lines indicate the angular positions of the reflexes of the solid solution $\text{Sr}_{0.75}\text{Ba}_{0.25}\text{Nb}_2\text{O}_6$ (PDF №73-487), the peaks of the polyniobate $\text{Ba}_4\text{SrNb}_4\text{O}_{15}$ (hereinafter SBNO_{15}) (PDF №54-1174) are indicated by an asterisk, and the reflexes of the substrate Al_2O_3 are indicated by a square.

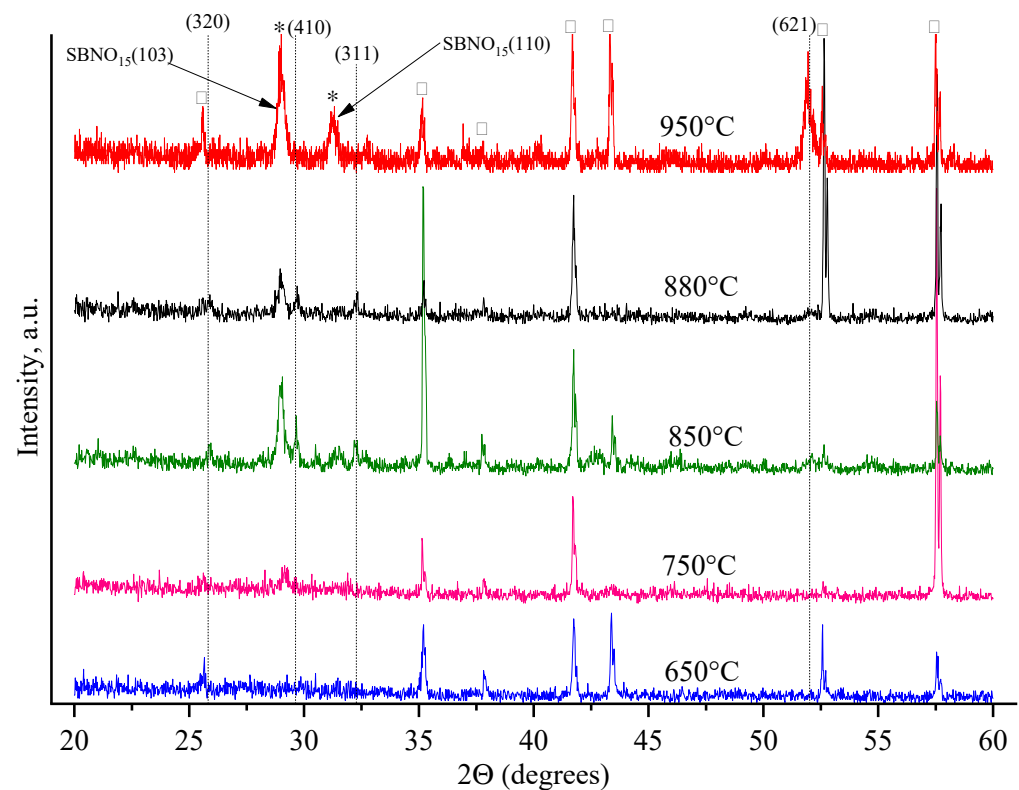


Figure 3. Diffractograms of as-deposited SBN thin films on alumina substrate; *—polyniobate $\text{Ba}_4\text{SrNb}_4\text{O}_{15}$; □—substrate Al_2O_3 .

At deposition temperatures of 650–750 °C, the formation of the SBN crystalline phase is practically not observed. With an increase in temperature to 850 °C, weak peaks of polycrystalline strontium barium niobate, as well as a reflex (103) from polyniobate SBNO_{15} of significant intensity in the region of 29°, appear. According to XRD analysis data, the main crystalline phase of films deposited on alumina at substrate temperatures below 850 °C is SBNO_{15} , which does not reveal ferroelectric properties. Stable formation of crystalline phases of SBN solid solution is observed at temperatures of 850 °C and above (high-temperature films hereinafter). On the diffractogram of the film deposited at $T_s = 850$ °C, peaks of weak intensity from strontium barium niobate appear that characterize the film as a pronounced polycrystal consisted of SBN and SBNO_{15} grains. Moreover, with a further increase in T_s , the ratio of SBN and SBNO_{15} phases changes towards the predominance of strontium barium niobate. It is known that the thermodynamics of crystallization of competing phases in the SBN system significantly depends on the temperature of the process [46]. The crystallization of secondary oxide phases such as SrNb_2O_6 or SNBO_{15} requires less thermal energy than the formation of a solid solution of SBN [47]. Moreover, the threshold thermal energy required to initiate the crystallization of SBN increases with increasing Sr content in the solid solution. This is confirmed by the data that show the solid solution $\text{Sr}_{0.75}\text{Ba}_{0.25}\text{Nb}_2\text{O}_6$ is less stable compared to solutions with a lower content of strontium [34].

The dynamics of the formation of crystalline phases in the studied films with an increase in the deposition temperature allows us to judge the high-temperature nature of the formation of a film solid solution of SBN on polycrystalline aluminum oxide in comparison with SBNO_{15} . It can be assumed that the large difference in the temperature coefficients of expansion of low-temperature SBNO_{15} and alumina leads to the appearance of cracks in the film, which is clearly visible in Figure 2a. Alternatively, being a higher-temperature phase, SBN is closer in terms of the temperature coefficient of expansion to alumina ($12 \times 10^{-6} \text{ K}^{-1}$ and $8 \times 10^{-6} \text{ K}^{-1}$, respectively) [48], which is manifested in improving the surface quality of the studied films with an increase in T_s (Figure 2b).

To improve the structural and dielectric characteristics of SBN thin films on alumina substrates, high-temperature annealing of samples was carried out at atmospheric pressure in air for an hour at a temperature of 1000 °C. All the studied SBN films were annealed in one step. Comparative diffractograms of films before and after annealing are presented in Figure 4.

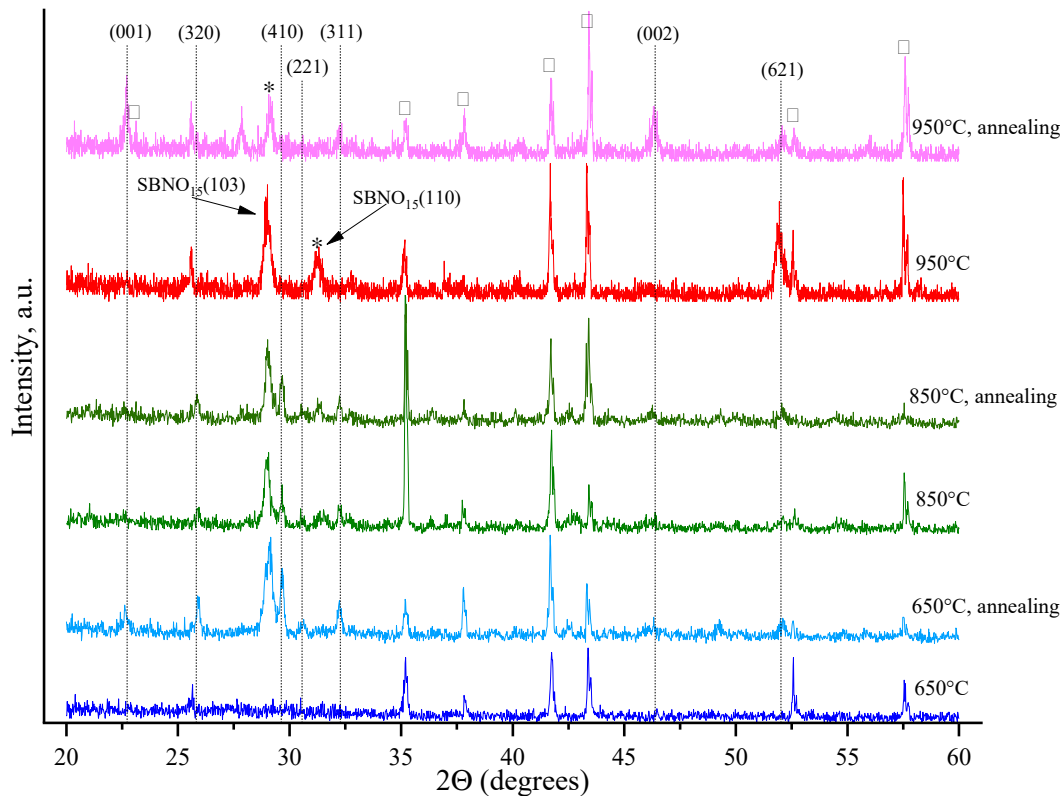


Figure 4. Diffractograms of SBN thin films obtained at 650–950 °C, before and after annealing at 1000 °C; *—polyniobate $\text{Ba}_4\text{SrNb}_4\text{O}_{15}$; □—substrate Al_2O_3 .

Annealing has a significantly different effect on the structure of films deposited at different substrate temperatures. Samples grown at T_s in the range of 650–850 °C exhibit, after annealing, a polycrystalline structure consisting of SBN grains of the (320), (410), and (311) orientations, with a predominance of SBNO_{15} crystallites of the (103) orientation. After annealing of the high-temperature film ($T_s = 950$ °C), on the contrary, both a decrease in the intensity of the peaks of the polyniobate at the angular positions 29° and 31.5° and recrystallization of the SBN grains of different orientations in the low surface energy (00 l) crystallites are observed. Thus, for all films, there is a significant change in the ratio of the SBN and SBNO_{15} phases after high-temperature treatment. This ratio can change both in the direction of increasing the content of the SBNO_{15} phase, as in the case of annealing the films deposited at $T_s < 850$ °C, and in the direction of increasing the content of the SBN phase, as in the case of annealing the films grown at $T_s > 850$ °C. It is obvious that the ratio of ferroelectric and linear dielectric phases in the film will determine both the nonlinear properties of the capacitor based on it and its microwave losses. An increase in the number of grains of the SBN phase and their (00 l) preferential orientation should have a positive effect on the tunable properties of the studied films.

3.3. Electrical Properties of SBN Planar Capacitive Structures

The dependence of the normalized capacitance on the control field strength for planar capacitors based on SBN films obtained at various T_s are presented in Figure 5. The measured capacitance values of the capacitors were 0.2–0.4 pF for various SBN films, which

corresponds to the values of the dielectric constant of 100–300 [49]. As expected, SBN films exhibit worse dielectric characteristics compared to bulk crystal or ceramics. Among the many factors leading to a decrease in the dielectric permittivity of SBN films discussed in the literature, the main ones are grain size distribution [33] and the effect of a defective layer on the film–substrate interface [32]. In our case, taking into account the island mechanism of growth of SBN films on alumina and the intensity and width of X-ray reflexes from the films, it can be concluded that the small size of crystalline grains and, consequently, a large number of grain boundaries are the main reasons for the deterioration of the dielectric properties of SBN films investigated compared to bulk material.

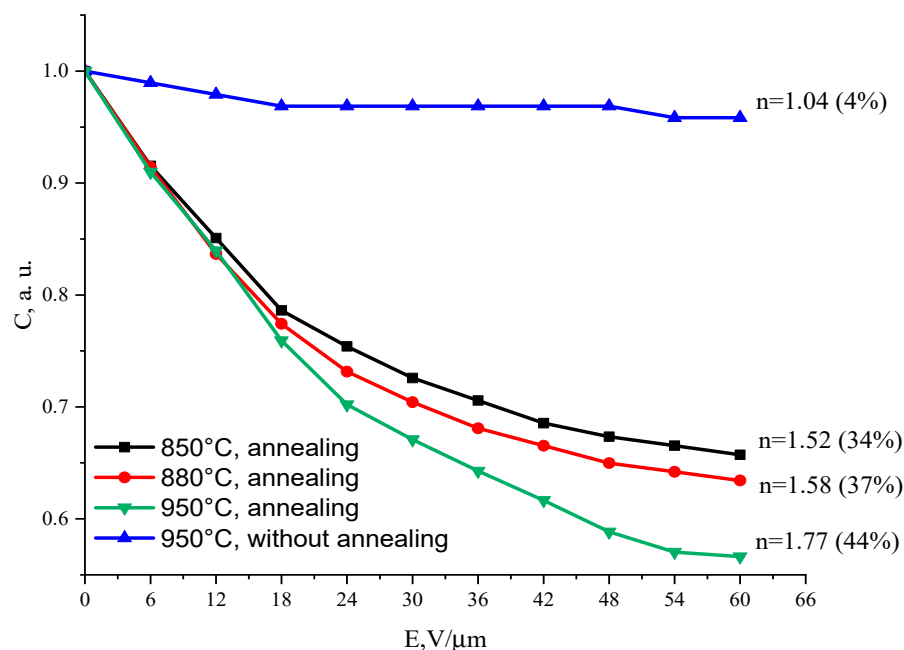


Figure 5. The dependence of the capacitance on the control field strength for planar capacitors based on SBN films obtained at various temperatures.

As for tunable properties, capacitors based on thin films grown at T_s of 650–750 °C do not reveal a change in capacitance under the action of the control field. The capacitor based on the high-temperature film without annealing reveals weak nonlinearity. Capacitive structures on the basis of films deposited at temperatures of 850 °C and 880 °C and subjected to high-temperature annealing exhibit tunability of the order of 1.5–1.6. The change in the capacitance under the influence of an external electric field for a planar capacitor based on the film grown at a temperature of 950 °C and subjected to annealing was $n = 1.77$ (44%), which can be explained by the (001) texture of this film.

The dependence of microwave losses on the control field strength for capacitors based on various SBN films is presented in Figure 6. As with the dependence of the capacitance vs. control field, three groups of curves can be considered: (i) the capacitor based on the SBN film without annealing does not exhibit dielectric nonlinearity at significant losses, which is explained by the presence of the SBNO_{15} phase and by a large number of structural defects in the film; (ii) capacitors based on films deposited at temperatures of 850 °C and 880 °C exhibit tunability of the order of 1.5 at losses of 0.05–0.025, explained by an increase in the volume of the SBN phase in the films as a result of annealing; and (iii) the capacitor based on the film grown at $T_s = 950$ °C and subjected to annealing demonstrates 44% tunability with a dielectric loss tangent of $\tan \delta = 0.009 \div 0.022$.

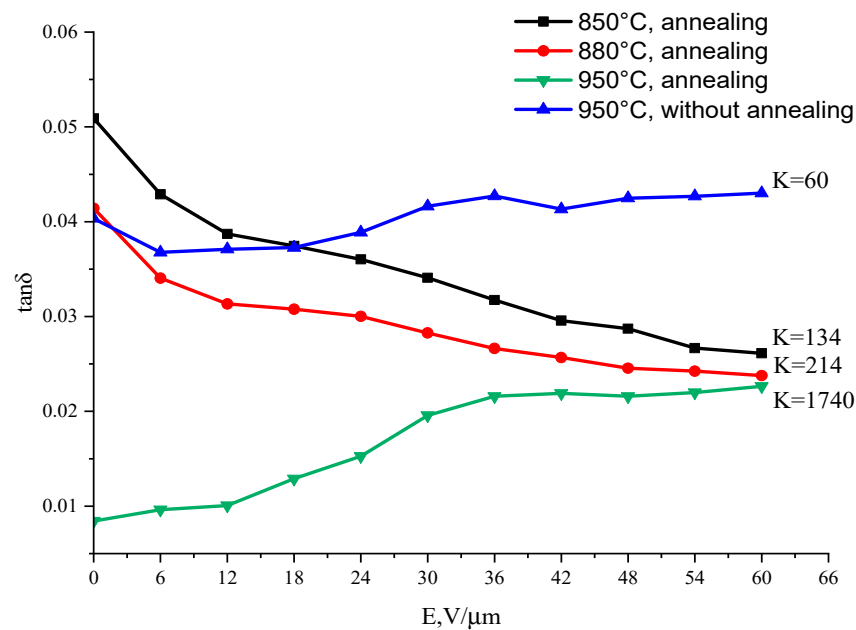


Figure 6. The dependence of microwave losses on the control field strength for capacitors based on various SBN films.

To compare capacitors, a commutation quality factor K is used, which is determined by the efficiency of changing the capacitance under the action of the control field and losses in the capacitor at zero and at maximum control field [50]:

$$K = \frac{(n - 1)^2}{n \cdot \tan \delta_1 \cdot \tan \delta_2},$$

where n is the tunability of the capacitor, and $\tan \delta_1$ and $\tan \delta_2$ are the losses of the capacitor at zero and maximum control field.

Table 3 presents comparative data on tunability and losses of capacitors based on SBN films on various substrates and in various electrode configurations (planar and plane-parallel structures) based on the literature data and on the results of this work.

Table 3. Comparative data on tunability and losses of capacitors based on SBN films.

Composition	Substrate	Design	Tunability, %	Losses, $\tan \delta$	K	Reference
$\text{Sr}_{0.5}\text{Ba}_{0.5}\text{Nb}_2\text{O}_6$	Pt/Si	MDM	18	not available	-	[32]
$\text{Sr}_{0.61}\text{Ba}_{0.39}\text{Nb}_2\text{O}_6$	MgO	planar	35	0.005–0.05 (12 GHz)	754	[9]
$\text{Sr}_{0.61}\text{Ba}_{0.39}\text{Nb}_2\text{O}_6$	LaAlO_3	planar	10	0.08–0.09 (1 MHz)	50	[38]
$\text{Sr}_{0.6}\text{Ba}_{0.4}\text{Nb}_2\text{O}_6$	Pt/Si	MDM	46	0.03–0.09 (10 kHz)	145	[34]
$\text{Sr}_{0.75}\text{Ba}_{0.25}\text{Nb}_2\text{O}_6$	Pt/Ti	MDM	45	0.034–0.036 (100 kHz)	300	[33]
$\text{Sr}_{0.75}\text{Ba}_{0.25}\text{Nb}_2\text{O}_6$	Al_2O_3	planar	44	0.009–0.022 (2 GHz)	1740	This work

It can be seen from the table that the planar capacitive structures obtained in this work reveal high dielectric nonlinearity at low losses, which is expressed in the quality factor $K = 1740$. According to [51], the device exhibits promising characteristics for microwave applications if the quality factor for it exceeds 1000. It should be noted that the planar capacitors based on SBN films on alumina substrate obtained in this work exhibit promising microwave characteristics in comparison with both MDM capacitors based on films grown on a platinum electrode and in comparison with planar structures on expensive single-crystal substrates. According to our data, this is the first successful attempt to form an SBN film on alumina with perspective microwave tunable characteristics acceptable for device applications.

4. Conclusions

SBN films of good crystallinity were grown on polycrystalline aluminum oxide substrate by magnetron sputtering for the first time. (00 l)-oriented films were obtained by deposition in oxygen atmosphere at a substrate temperature of 950 °C with post-growth annealing in air. The structure, phase, and elemental composition of the obtained films were investigated by methods of scattering medium-energy ions, X-ray diffraction analysis, and electron microscopy. According to X-ray diffraction analysis, the main crystalline phase of films deposited on alumina at substrate temperatures below 850 °C is SBNO₁₅ polyniobate, which does not have ferroelectric properties. Stable formation of crystalline phases of SBN solid solution is observed at temperatures of 850 °C and above. The dynamics of the growth of crystalline phases in the studied films with an increase in the deposition temperature shows the high-temperature nature of the formation of a film solid solution of SBN on polycrystalline aluminum oxide in comparison with secondary oxides of the SBN system. The tunability and microwave losses of SBN planar capacitors is shown to be correlated with the volume fraction of the SBN phase in the film determined by the deposition temperature and annealing conditions. The capacitor based on the SBN film deposited at a temperature of 950 °C and subjected to annealing demonstrates a tunability of 44% and a loss tangent of $0.009 \div 0.022$ at 2 GHz, which is expressed in quality factor $K = 1740$. This is the first successful attempt to form planar capacitive structures based on SBN films on polycrystalline aluminum oxide, which reveal the commutation quality factor above 1000, suitable for tunable microwave applications.

Author Contributions: Conceptualization, A.T. and L.I.; methodology, A.T.; software, I.S. and V.S.; validation, A.T., A.B. and E.S.; formal analysis, A.B., E.S., A.G. and L.I.; investigation, A.T., A.B., E.S., L.I., I.S., A.G. and V.S.; resources, A.T., I.S. and V.S.; data curation, A.T., A.B., I.S. and V.S.; writing—original draft preparation, A.B.; writing—review and editing, A.T., L.I. and A.B.; visualization, A.B. and E.S.; supervision, A.T. and L.I.; project administration, A.T.; funding acquisition, A.T. All authors have read and agreed to the published version of the manuscript.

Funding: The work was supported by the Russian Science Foundation under grant No. 23-29-00757. Igor Serenkov and Vladimir Sakharov worked independently of grant support.

Institutional Review Board Statement: Not applicable.

Informed Consent Statement: Not applicable.

Data Availability Statement: Data are contained within the article.

Acknowledgments: The authors thank Almjashev Vyacheslav from the Saint Petersburg Electrotechnical University "LETI" for SEM measurements.

Conflicts of Interest: The authors declare no conflict of interest.

References

1. Martin, L.W.; Rappe, A.M. Thin-film ferroelectric materials and their applications. *Nat. Rev. Mater.* **2016**, *2*, 16087. [[CrossRef](#)]
2. Kong, L.B.; Li, S.; Zhang, T.S.; Zhai, J.W.; Boey, F.C.; Ma, J. Electrically tunable dielectric materials and strategies to improve their performances. *Prog. Mater. Sci.* **2010**, *55*, 840–893. [[CrossRef](#)]
3. Liu, X.; Tu, J.; Li, H.; Tian, J.; Zhang, L. Research progress of double perovskite ferroelectric thin films. *Appl. Phys. Rev.* **2023**, *10*, 021315. [[CrossRef](#)]
4. Song, L.; Glinsek, S.; Defay, E. Toward low-temperature processing of lead zirconate titanate thin films: Advances, strategies, and applications. *Appl. Phys. Rev.* **2021**, *8*, 041315. [[CrossRef](#)]
5. Daumont, C.J.M.; Simon, Q.; Le Mouellic, E.; Payan, S.; Gardes, P.; Poveda, P.; Wolfman, J. Tunability, dielectric, and piezoelectric properties of Ba_(1-x)Ca_xTi_(1-y)Zr_yO₃ ferroelectric thin films. *J. Appl. Phys.* **2016**, *119*, 094107. [[CrossRef](#)]
6. Zhang, H.; Giddens, H.; Saunders, T.G.; Palma, M.; Abrahams, I.; Yan, H.; Hao, Y. Microwave tunability in tin substituted barium titanate. *J. Eur. Ceram. Soc.* **2023**, *in press*. [[CrossRef](#)]
7. Huang, J.; Gao, X.; MacManus-Driscoll, J.L.; Wang, H. Ferroelectric thin films and nanostructures: Current and future. In *Nanostructures in Ferroelectric Films for Energy Applications*; Elsevier: Amsterdam, The Netherlands, 2019; pp. 19–39.
8. Alema, F.; Pokhodnya, K. Dielectric properties of BaMg_{1/3}Nb_{2/3}O₃ doped Ba_{0.45}Sr_{0.55}TiO₃ thin films for tunable microwave applications. *J. Adv. Dielectr.* **2015**, *5*, 1550030. [[CrossRef](#)]

9. Moon, S.E.; Kwak, M.H.; Kim, Y.T.; Ryu, H.C.; Lee, S.J.; Kang, K.Y. Measurement of microwave dielectric properties of (Sr,Ba)Nb₂O₆ thin films. *Integr. Ferroelectr.* **2004**, *66*, 275–281. [[CrossRef](#)]
10. Nguyen, M.D.; Tran, D.T.; Dang, H.T.; Nguyen, C.T.Q.; Rijnders, G.; Vu, H.N. Relaxor-Ferroelectric Films for Dielectric Tunable Applications: Effect of Film Thickness and Applied Electric Field. *Materials* **2021**, *14*, 6448. [[CrossRef](#)]
11. Zhao, Q.; Yan, Z.; Chen, C.; Chen, J. Spinels: Controlled preparation, oxygen reduction/evolution reaction application, and beyond. *Chem. Rev.* **2017**, *117*, 10121–10211. [[CrossRef](#)]
12. Tumarkin, A.; Sapego, E.; Gagarin, A.; Karamov, A. High Tunable BaTi_xZr_{1-x}O₃ Films on Dielectric Substrate for Microwave Applications. *Molecules* **2022**, *27*, 6086. [[CrossRef](#)]
13. Zhang, W.; Hu, F.; Zhang, H.; Ouyang, J. Investigation of the electrical properties of RF sputtered BaTiO₃ films grown on various substrates. *Mater. Res. Bull.* **2017**, *95*, 23–29. [[CrossRef](#)]
14. Wollesen, L.; Douissard, P.A.; Infante, I.C.; Margueritat, J.; Gautier, B.; Martin, T.; Dujardin, C. Tunable crystalline structure and electrical properties of (Pb,Sr)TiO₃ films grown by liquid phase epitaxy. *CrystEngComm* **2023**, *25*, 2096–2103. [[CrossRef](#)]
15. Choueikani, F.; Jamon, D.; Neveu, S.; Blanc-Mignon, M.F.; Lefkir, Y.; Royer, F. Self-biased magneto-optical films based on CoFe₂O₄-silica nanocomposite. *J. Appl. Phys.* **2021**, *129*, 023101. [[CrossRef](#)]
16. Zhao, H.; Ning, X.; Yao, H.; Hao, A.; Ismail, M. Facile sol-gel method derived Au nanoparticles decoration nickel ferrites thin films: Effect on optical and magnetic properties. *Mater. Chem. Phys.* **2021**, *265*, 124480. [[CrossRef](#)]
17. Jackson, T.J.; Jones, I.P. Nanoscale defects and microwave properties of (BaSr)TiO₃ ferroelectric thin films. *J. Mater. Sci.* **2009**, *44*, 5288–5296. [[CrossRef](#)]
18. Zhang, Y.J.; Zheng, X.J.; Jiao, F.; Hu, H.P. The effect of strain and dead layer on the nonlinear electric-mechanical behavior of ferroelectric thin films. *Comput. Mater. Sci.* **2013**, *77*, 377–383. [[CrossRef](#)]
19. Roytburd, A.L.; Ouyang, J.; Artemev, A. Polydomain structures in ferroelectric and ferroelastic epitaxial films. *J. Phys. Condens. Matter* **2017**, *29*, 163001. [[CrossRef](#)]
20. Nguyen, P.T.; Nguyen, T.; Nguyen, M.D.; Vu, T.H. Impact of electrode materials on microstructure, leakage current and dielectric tunable properties of lead-free BSZT thin films. *Ceram. Int.* **2021**, *47*, 23214–23221. [[CrossRef](#)]
21. Xu, Y. *Ferroelectric Materials and Their Applications*; Elsevier: Amsterdam, The Netherlands, 2013.
22. Tumarkin, A.; Sapego, E.; Gagarin, A.; Senkevich, S. Enhanced tunability of BaTi_xSn_{1-x}O₃ films on dielectric substrate. *Appl. Sci.* **2021**, *11*, 7367. [[CrossRef](#)]
23. Dhole, S.; Chen, A.; Nie, W.; Park, B.; Jia, Q. Strain engineering: A pathway for tunable functionalities of perovskite metal oxide films. *Nanomaterials* **2022**, *12*, 835. [[CrossRef](#)] [[PubMed](#)]
24. Raeder, T.M.; Holstad, T.S.; Nylund, I.E.; Einarsrud, M.A.; Glaum, J.; Meier, D.; Grande, T. Anisotropic in-plane dielectric and ferroelectric properties of tensile-strained BaTiO₃ films with three different crystallographic orientations. *AIP Adv.* **2021**, *11*, 025016. [[CrossRef](#)]
25. Wang, J.; Lou, J.; Wang, J.F.; Qu, S.B.; Du, H.L.; Cui, T.J. Ferroelectric composite artificially-structured functional material: Multifield control for tunable functional devices. *J. Phys. D Appl. Phys.* **2022**, *55*, 303002. [[CrossRef](#)]
26. Tumarkin, A.; Gagarin, A.; Odinets, A.; Zlygostov, M.; Sapego, E.; Kotelnikov, I. Structural and microwave characterization of BaSrTiO₃ thin films deposited on semi-insulating silicon carbide. *Jpn. J. Appl. Phys.* **2018**, *57*, 11UE02. [[CrossRef](#)]
27. Harris, D.T.; Lam, P.G.; Burch, M.J.; Li, J.; Rogers, B.J.; Dickey, E.C.; Maria, J.P. Ultra-high tunability in polycrystalline Ba_{1-x}Sr_xTiO₃ thin films. *Appl. Phys. Lett.* **2014**, *105*, 072904. [[CrossRef](#)]
28. Razumov, S.; Tumarkin, A.; Gaidukov, M.; Gagarin, A.; Kozyrev, A.; Vendik, O.; Ivanov, A.; Buslov, O.; Keys, V.; Sengupta, L.C.; et al. Characterisation of quality of Ba_xSr_{1-x}TiO₃ thin film by the commutation quality factor measured at microwaves. *Appl. Phys. Lett.* **2002**, *81*, 1675–1677. [[CrossRef](#)]
29. Kaushal, A.; Vardhan, A.; Rawat, R.S.S. Intelligent material for modern age: A review. *IOSR J. Mech. Civ. Eng.* **2016**, *13*, 10–15.
30. He, H.; Lu, X.; Hanc, E.; Chen, C.; Zhang, H.; Lu, L. Advances in lead-free pyroelectric materials: A comprehensive review. *J. Mater. Chem. C* **2020**, *8*, 1494–1516. [[CrossRef](#)]
31. Jindal, S.; Vasishth, A.; Devi, S.; Anand, G. A review on tungsten bronze ferroelectric ceramics as electrically tunable devices. *Integr. Ferroelectr.* **2018**, *186*, 1–9. [[CrossRef](#)]
32. Cheng, H.F.; Chiou, G.S.; Liu, K.S.; Lin, I.N. Ferroelectric properties of (Sr_{0.5}Ba_{0.5})Nb₂O₆ thin films synthesized by pulsed laser deposition. *Appl. Surf. Sci.* **1997**, *113*, 217–221. [[CrossRef](#)]
33. De Los, S.; Guerra, J.; Mendes, R.G.; Eiras, J.A.; Santos, I.A.; Araujo, E.B. Investigation of nonlinear dielectric properties in Sr_{0.75}Ba_{0.25}Nb₂O₆ relaxor ferroelectric thin films. *J. Appl. Phys.* **2008**, *103*, 014102. [[CrossRef](#)]
34. Boulay, N.; Cuniot-Ponsard, M.; Desvignes, J.M.; Bellemain, A. Dielectric and ferroelectric properties of Sr_xBa_{1-x}Nb₂O₆ (SBN: X) thin films. *Ferroelectrics* **2007**, *353*, 10–20. [[CrossRef](#)]
35. Beskin, I.M.; Kwon, S.; Posadas, A.B.; Kim, M.J.; Demkov, A.A. Growth and structure of strong pockels material strontium barium niobate on SrTiO₃ and Si by molecular beam epitaxy. *Adv. Photonics Res.* **2021**, *2*, 2100111. [[CrossRef](#)]
36. Pedersen, V.H.; Blichfeld, A.B.; Bakken, K.; Chernyshov, D.; Grande, T.; Einarsrud, M.A. Crystallization and texturing of Sr_xBa_{1-x}Nb₂O₆ thin films prepared by aqueous solution deposition—An in-situ X-ray diffraction study. *Cryst. Growth Des.* **2022**, *22*, 5912–5922. [[CrossRef](#)]
37. Tumarkin, A.; Razumov, S.; Gagarin, A.; Altyinnikov, A.; Mikhailov, A.; Platonov, R.; Butler, J.E. Ferroelectric varactor on diamond for elevated power microwave applications. *IEEE Electron Device Lett.* **2016**, *37*, 762–765. [[CrossRef](#)]

38. Rodríguez-Santiago, V.; González, Y.; Fernández, F.E.; Mueller, C.H.; Keuls, F.W.V.; Miranda, F.A. Microwave properties of strontium barium niobate thin films grown by pulsed laser deposition. *MRS Online Proc. Libr.* **2001**, *688*, 7121. [[CrossRef](#)]
39. Setter, N.; Damjanovic, D.; Eng, L.; Fox, G.; Gevorgian, S.; Hong, S.; Streiffer, S. Ferroelectric thin films: Review of materials, properties, and applications. *J. Appl. Phys.* **2006**, *100*, 051606. [[CrossRef](#)]
40. Schmelzer, J.W. *Nucleation Theory and Applications*; Strauss GmbH: Mörlenbach, Germany, 2004.
41. Tumarkin, A.V.; Serenkov, I.T.; Sakharov, V.I.; Afrosimov, V.V.; Odinets, A.A. Influence of the substrate temperature on the initial stages of growth of barium strontium titanate films on sapphire. *Phys. Solid State* **2016**, *58*, 364–369. [[CrossRef](#)]
42. Kukushkin, S.A.; Osipov, A.V. Theory of phase transformations in the mechanics of solids and its applications for description of fracture, formation of nanostructures and thin semiconductor films growth. *Key Eng. Mater.* **2013**, *528*, 145–164. [[CrossRef](#)]
43. Kukushkin, S.A.; Osipov, A.V. Nucleation kinetics of nanofilms. In *Encyclopedia of Nanoscience and Nanotechnology*; American Scientific Publishers: Valencia, CA, USA, 2004; Volume 8, pp. 113–136.
44. Kukushkin, S.A. Evolution processes in multicomponent and multiphase films. *Thin Solid Film.* **1992**, *207*, 302–312. [[CrossRef](#)]
45. Tumarkin, A.V.; Serenkov, I.T.; Sakharov, V.I. Investigation of the initial stages of the growth of barium strontium titanate ferroelectric films by medium-energy ion scattering. *Phys. Solid State* **2010**, *52*, 2561–2564. [[CrossRef](#)]
46. Lukasiewicz, T.; Swirkowicz, M.A.; Dec, J.; Hofman, W.; Szyrski, W. Strontium–barium niobate single crystals, growth and ferroelectric properties. *J. Cryst. Growth* **2008**, *310*, 1464–1469. [[CrossRef](#)]
47. Cuniot-Ponsard, M.; Desvignes, J.M.; Leroy, E. RF Magnetron Sputtering Deposition of Hetero-Epitaxial $\text{Sr}_x\text{Ba}_{1-x}\text{Nb}_2\text{O}_6$ Thin Films: The Role of Temperature. *Ferroelectrics* **2003**, *288*, 159–168. [[CrossRef](#)]
48. Paszkowski, R.; Wokulska, K.; Dec, J. Thermal expansion coefficients of strontium-barium niobate single crystals in the vicinity of the phase transition point. *Cryst. Res. Technol.* **2017**, *52*, 1600368. [[CrossRef](#)]
49. Vendik, O.G.; Zubko, S.P.; Nikol'Skii, M.A. Modeling and calculation of the capacitance of a planar capacitor containing a ferroelectric thin film. *Tech. Phys.* **1999**, *44*, 349–355. [[CrossRef](#)]
50. Vendik, I.B.; Vendik, O.G.; Kollberg, E.L. Commutation quality factor of two-state switchable devices. *IEEE Trans. Microw. Theory Tech.* **2000**, *48*, 802–808. [[CrossRef](#)]
51. Vendik, O.G. Ferroelectrics find their “niche” among microwave control devices. *Phys. Solid State* **2009**, *51*, 1529–1534. [[CrossRef](#)]

Disclaimer/Publisher’s Note: The statements, opinions and data contained in all publications are solely those of the individual author(s) and contributor(s) and not of MDPI and/or the editor(s). MDPI and/or the editor(s) disclaim responsibility for any injury to people or property resulting from any ideas, methods, instructions or products referred to in the content.